

---

# Context and Diversity Matter: The Emergence of In-Context Learning in World Models

---

\*†Fan Wang<sup>1,2</sup>, \*Zhiyuan Chen<sup>1</sup>, \*Yuxuan Zhong<sup>1</sup>, Sunjian Zheng<sup>1</sup>, Pengtao Shao<sup>1</sup>, Bo Yu<sup>1</sup>,  
†Shaoshan Liu<sup>1</sup>, Jianan Wang<sup>3</sup>, Ning Ding<sup>1</sup>, Yang Cao<sup>2</sup>, and Yu Kang<sup>2</sup>

<sup>1</sup>Shenzhen Institute of Artificial Intelligence and Robotics for Society, Shenzhen, China

<sup>2</sup>University of Science and Technology of China, Hefei, China

<sup>3</sup>Astribot, Shenzhen, China

## Abstract

The capability of predicting environmental dynamics underpins both biological neural systems and general embodied AI in adapting to their surroundings. Yet prevailing approaches rest on static world models that falter when confronted with novel or rare configurations. We investigate in-context environment learning (ICEL), shifting attention from zero-shot performance to the growth and asymptotic limits of the world model. Our contributions are three-fold: (1) we formalize in-context learning of a world model and identify two core mechanisms: environment recognition and environment learning; (2) we derive error upper-bounds for both mechanisms that expose how the mechanisms emerge; and (3) we empirically confirm that distinct ICL mechanisms exist in the world model, and we further investigate how data distribution and model architecture affect ICL in a manner consistent with theory♣. These findings demonstrate the potential of self-adapting world models and highlight the key factors behind the emergence of ICEL, most notably the necessity of long context and diverse environments.

## 1 Introduction

The ability to predict future environmental states is crucial for reasoning and decision-making in both animals and humans. Inspired by this principle, constructing predictive models, especially the world model [1], to forecast environmental dynamics and outcomes forms the foundation for enabling agents to plan effective decisions and behaviors [2–6]. Consequently, world models are widely applied in fields such as navigation [7–11], autonomous driving [12–16], robotics [17–22], and are considered a cornerstone of embodied artificial intelligence.

Despite their proven effectiveness across various applications, previous prediction frameworks largely rely on static world models optimized for zero-shot, few-shot, or instantaneous performance. In contrast, humans and animals achieve real-time adaptation [23] through predictive coding—a process where prediction errors drive attention, generate feedback, and motivate learning and adjustment [24, 25]. For instance, when confronted with rare environments, humans experience surprise yet rapidly recalibrate their predictions for that setting, whereas static models continue to fail unless explicitly retrained on the relevant data. The ability to dynamically modify predictive mechanisms based on observational evidence, rather than relying solely on fixed parametric memory and external mapping modules, can effectively enable the model to adapt to environments unseen during training. This capability can be effectively addressed by In-Context Learning (ICL), as evidenced by recent advances

---

\*Equal Contribution

†Corresponding to: fanwang.px@gmail.com, shaoshanliu@cuhk.edu.cn

♣Source code: <https://github.com/airs-cuhk/airsoul/tree/main/projects/MazeWorld>

in Large Language Models [26]. However, the potential of ICL for resolving plasticity in world models, particularly In-Context Environment Learning (ICEL), remains largely underexplored in current literature. Addressing this gap could further improve the generalization scope for embodied AI.

We isolate two canonical mechanisms that let world models adapt in context. In-Context Environment Recognition (ICER) taps the model’s parametric memory of previously seen environments and uses the context only to identify which one is active. ICEL ignores prior settings and instead extracts the full environment from the context itself. By deriving error bounds for both modes, we show how their emergence depends on data distribution, including environment diversity, complexity, and trajectory length. To test the theory, we introduce **Linear-attention Long-context world** model, *L2World*, which effectively model long sequences with high computational efficiency. Across cart-pole control and vision-based indoor navigation, we find that distributional properties and long-context capacity govern whether the model invokes ICER or ICEL. Despite the light image encoders and decoders of *L2World*, it sets a new state-of-the-art for long-sequence observation prediction in navigation, outperforming approaches that rely on heavy diffusion-based image backbones. These results underscore the importance and the promise of deliberately incentivizing ICEL through carefully designed datasets and model architectures to strengthen the asymptotic generalization capability of world models, rather than focusing solely on instant or zero-shot frame-level performance.

## 2 Related Work

### 2.1 Dynamic Prediction and World Models

Dynamic models, also referred to as world models [1, 27], encompass probabilistic, physical, or generative frameworks that formalize an AI system’s environmental understanding [28–31]. These models predict future states by leveraging historical observations and play a pivotal role in advancing reinforcement learning (RL) methodologies and related domains. Specifically, they constitute foundational components in model-based RL [32, 33], enable simulations that facilitate agent learning through virtual experiences (thereby reducing reliance on direct environmental interaction) [34, 2, 5, 35, 36], and serve as auxiliary tasks to augment model supervision [37–39].

World models demonstrate robustness in integrating multi-modal raw sensor data, including visual, textual, inertial, and tactile inputs. To mitigate challenges posed by high-dimensional sensory inputs, representation learning paradigms such as Generative Adversarial Networks (GANs) [40] and Variational Autoencoders (VAEs) [41] are widely utilized to compress raw data into compact latent spaces. Subsequent temporal modeling in these reduced dimensions is achieved through latent world model architectures [2, 42, 4, 5, 43, 39, 44, 45], which capture sequential dependencies and enable coherent long-term predictions.

In navigation, early systems relied on traditional, hand-crafted pipelines such as SLAM. Recent work replaces these modules with generative world models, including diffusion [7], VAE [9], and RL-enhanced variants [46, 10], which reconstruct dynamics or simulate semantics [47, 48]. However, most existing methods disregard continual adaptation, especially across episodes, leaving a persistent gap between zero-shot performance and lifelong operation.

### 2.2 In-Context Learning and Meta-Learning

The approach based on parametric memory, which predominantly relies on gradient-based optimization or In-Weight Learning (IWL), has faced criticism for its lack of plasticity and the associated challenges it poses in continual learning scenarios [49]. Conversely, ICL has emerged as a pivotal capability in large language models [26], facilitating generalization to novel tasks without the necessity of parameter fine-tuning. ICL leverages contextual memory for task solutions, rather than depending on parametric memory. The concept of ICL is not novel. Meta-learning [50, 51], which focuses on acquiring learning capabilities rather than mastering specific skills, utilizes well-curated environments or data instead of relying on large-scale, uncurated pre-training data. Nevertheless, the lack of well-structured, task-rich, and cost-efficient datasets continues to present a significant challenge.

ICL has been utilized to encode a diverse array of learning mechanisms, including language learning [52], regression [53], Bayesian inference [54], reinforcement learning [55–57], and world mod-

els [58, 59], highlighting its resemblance to biological plasticity [60]. Yet existing work concentrates on few-shot in-context adaptation, overlooking ICL’s potential as contexts grow indefinitely. Moreover, little insight has been offered into its inner process and mechanisms. Concurrent studies identify at least two ICL modes in LLMs: task recognition (TR) and task learning (TL) [61]. Key factors conducive to ICL emergence have also been investigated [62, 58], such as “burstiness” and diversity, and so is the relation between IWL and ICL [63], but theory in this area remains under-developed.

### 3 Methodologies

We consider an environment  $e$  specified by a Partially Observable Markov Decision Process (POMDP)  $e : \langle O, S, A, T_e, Z_e \rangle$ , where  $S$  is the state space,  $A$  is the action space,  $O$  is the observation space,  $T_e(s, a, s') = p_{\tau,e}(s'|s, a)$  is the transition model, and  $Z_e(s, o) = p_{z,e}(o|s)$  is the observation model.

<sup>1</sup> A fully observable MDP is denoted with  $e : \langle S, A, T_e \rangle$  with  $o \equiv s$ . We denote a world model with the following equation:

$$\begin{aligned} \text{World Model: } \hat{o}_{t+1} \sim \hat{p}_\theta(\cdot|q_t) = f_\theta(q_t), \text{ with } q_t = (s_t, a_t) \text{ (MDP)} \\ \text{or } q_t = (o_{t-\Delta t}, a_{t-\Delta t}, \dots, o_t, a_t) \text{ (POMDP)}. \end{aligned} \quad (1)$$

Let  $\theta$  denote the model parameters; values marked with a hat denote predictions, and unmarked values denote the ground truth. Consider extra contexts of observations and actions,  $C_T = (o_1^{(C)}, a_1^{(C)}, \dots, o_T^{(C)}, a_T^{(C)})$ , where  $T$  indexes the context length; the ICL capability of the world model is then characterized by the following condition:

$$\forall T_1 > T_2, D[\hat{p}_\theta(\cdot|q_t, C_{T_1}) || p_e(\cdot|q_t)] < D[\hat{p}_\theta(\cdot|q_t, C_{T_2}) || p_e(\cdot|q_t)], \quad (2)$$

Here,  $D$  represents a metric measuring the error between two distributions (lower values indicate better performance). Notably, the ICL of the world model fundamentally relies on cross-episode contexts rather than intra-episode state estimation. To distinguish these concepts clearly, we use  $q_t$  to denote short-term state estimation and  $C_T$  to represent long-term ICL. While these are typically aligned in a single sequence in practice, maintaining this distinction facilitates rigorous theoretical analysis. Building on prior work that partitions in-context learning into task-recognition (TR) and task-learning (TL) modes [61, 64], theoretically, we are able to identify two analogous modes within world-model ICL: *Environment Recognition* (ER) and *Environment Learning* (EL). We then derive error bounds that characterize the conditions under which each mode emerges.

#### 3.1 Environment Recognition (ER)

To clarify Equation (2), we consider a world model optimized on the finite environment set  $\mathcal{E} = \{e_1, \dots, e_{|\mathcal{E}|}\}$ . Assume the system possesses an environment-specific model  $\hat{p}_{\theta,e}$  for every environment  $e$ , then  $\hat{p}_\theta$  decomposes as follows:

$$\begin{aligned} \hat{p}_{\theta,ER}(o_{t+1}|q_t, C_T) &= \sum_{e \in \mathcal{E}} \underbrace{\hat{p}_\theta(e|q_t, C_T)}_{\text{Environment Recognition}} \cdot \underbrace{\hat{p}_{\theta,e}(o_{t+1}|q_t)}_{\text{Environment-Specific World Model}} \quad (3) \\ \hat{p}_{\theta,e}(o_{t+1}|q_t) &= \int \underbrace{\hat{p}_{\theta,s,e}(s_t|q_t)}_{\text{State Estimation}} \cdot \underbrace{\hat{p}_{\theta,\tau,e}(s_{t+1}|s_t, a_t)}_{\text{Dynamics}} \cdot \underbrace{\hat{p}_{\theta,z,e}(o_{t+1}|s_{t+1})}_{\text{Observation Model}} ds_t \end{aligned}$$

Equation (3) implies that in-context learning in world models arises mainly from the continual refinement of environment recognition, since the context yields no improvement to the environment-specific world-model term  $\hat{p}_{\theta,e} = \{\hat{p}_{\theta,s,e}, \hat{p}_{\theta,\tau,e}, \hat{p}_{\theta,z,e}\}$ . Therefore, in the ER regime, the model first acquires world models for the entire environment set through IWL or parametric memory, and then uses the context solely to identify the current environment.

#### 3.2 Environment Learning (EL)

Equation (3) is efficient when the environment set  $\mathcal{E}$  is small, yet its effectiveness diminishes rapidly as the size and diversity of  $\mathcal{E}$  grow or when the system faces open worlds. However  $\hat{p}_\theta$  can also be

<sup>1</sup>While most prior work integrates the reward model into the world model, our analyses omit explicit consideration of rewards. Nonetheless, since rewards can typically be derived from the state or observation, our framework allows for straightforward extension to incorporate reward-related considerations.

approximated without estimating  $e$  at all, by directly accumulating the evidence for  $(q_t, o_{t+1})$  across all contexts:

$$\hat{p}_{\theta, EL}(o_{t+1}|q_t, C_T) = \frac{p(q_t, o_{t+1}|C_T)}{p(q_t|C_T)} \quad (4)$$

An intuitive observation of Equation (4) is that EL functions, at minimum, as a in-context memorizer. For highly complex environments, its performance might degrade sharply, because accurate estimation of the transition of  $q_t$  demands contexts that scale with the environment’s complexity.

### 3.3 Theoretical Analyses of ER and EL

Although the training process and data distribution play a key role in effectively incentivizing ICL [62], how does the data distribution determine whether EL or ER emerges? If training consistently minimizes predictive error, the error bounds of EL and ER become the decisive factor in selecting the emergent mode. To investigate the conditions governing the emergence of the two modes (ER and EL), we analyze the error upper bounds for each paradigm. For tractable analysis, we introduce the following simplifying assumptions: (1) The observation, state, and action spaces are discrete; (2) Both modes achieve ideal state estimation  $p_e(s|q)$ ; (3) The context  $C_T$  has a uniform state-action distribution. Under these assumptions, we derive an upper bound on the error of the world model optimized over environment set  $\mathcal{E}$ , measured by the total variation (TV) distance, when deployed in an unseen environment  $e_0$  at context horizon  $T$ . Formally, the TV error is bounded by:

**Theorem 1.** *For Environment Recognition and Environment Learning whose predictive models  $\hat{p}_{ER/EL}$  have been sufficiently optimized on the training environments  $\mathcal{E}$ , the upper bound of the total-variation (TV) distance between the predicted and the ground-truth transition, given a context  $C_T$  of length  $T$ , can be estimated as:*

$$\begin{aligned} TV(\hat{p}_{ER}, p_{e_0}) &\leq \underbrace{\min\{\alpha(|\mathcal{E}| - 1)T^{-1/2}/3\}}_{\text{Identification Error}} + \underbrace{\min_{e \in \mathcal{E}} TV(\hat{p}_{\theta, e}, p_{e_0})}_{\text{Best Matching Error}}, & \underbrace{\max_{e \in \mathcal{E}} TV(\hat{p}_{\theta, e}, p_{e_0})}_{\text{Worst Matching Error}} \\ TV(\hat{p}_{EL}, p_{e_0}) &\leq \underbrace{\sqrt{2|O||S||A|\log(4|O|/\delta)}}_{\text{Environment Complexity}} \cdot T^{-1/2}, \\ &\text{with probability } 1 - \delta, \text{ and } T > 4|S|^2|A|^2 \log(4|S||A|/\delta) \end{aligned} \quad (5)$$

Proofs and detailed assumptions for the above theorems are deferred to Section A. An immediate observation from Theorem 1 is that ICER enjoys an ideal error upper bound that decays as  $T^{-1/2}$ , whereas ICER carries a non-decaying residual term (the best-matching error) that becomes the dominant obstacle to generalizing across unseen environments. To enhance generalization, we therefore ask: under what condition is ICER preferred to ICER? For the entire training set  $\mathcal{E}$ , ICER dominates whenever  $\mathbb{E}_{e \in \mathcal{E}} [TV(\hat{p}_{EL}, p_e)] \ll \mathbb{E}_{e \in \mathcal{E}} [TV(\hat{p}_{ER}, p_e)]$ ; The opposite inequality favors ICER. Although the errors themselves are intractable to evaluate directly, the following insights are obtained by comparing their upper bounds:

- (1) **Lower environment complexity and greater environment diversity favor EL over ER:** Note that the best-matching error is effectively zero, because the model is always evaluated on environments seen during training. The cardinality of the training set,  $|\mathcal{E}|$ , enters only the ER bound, whereas the environment complexity,  $|O||S||A|$ , enters only the EL bound. Consequently, lower complexity and a larger training set push the EL bound below the ER bound. Moreover, because ER error is limited by the worst-matching error, scarce diversity in the training environments can keep the ER error small and prevent EL from ever overtaking it.
- (2) **Long context and environment diversity are key to both ER and EL:** Insufficient diversity not only blocks the emergence of ICER but also suppresses ICER, because a small worst-matching error removes the pressure to reduce the identification error. Once the training set is sufficiently diverse, both ER and EL obtain an upper error bound that decays as  $T^{-1/2}$ , demonstrating that long context is indispensable for either mechanism.
- (3) **Over-training and powerful IWL facilitate ER over EL:** we hypothesize that IWL perfectly models the environment-specific dynamics  $(\hat{p}_{\theta, e})$  in the training set, so the best-matching error is nearly zero during training; however, this is not always true. Early in training, IWL can still incur large

errors, transiently pushing the model toward EL instead of ER. This transiency is also investigated by prior works in ICL [65]. As training proceeds and IWL becomes increasingly accurate, the model may revert to ER.

In the following section, we empirically confirm that these insights hold not only for discrete settings but also for continuous MDPs and POMDPs. Because theory predicts that large environmental diversity and low task complexity are required for incentivizing EL, and most of the closed benchmarks can not satisfy those requirements. We construct our dataset from randomly sampled *cart-poles* and procedurally generated *mazes* to evaluate the performance of ICER and ICEL.

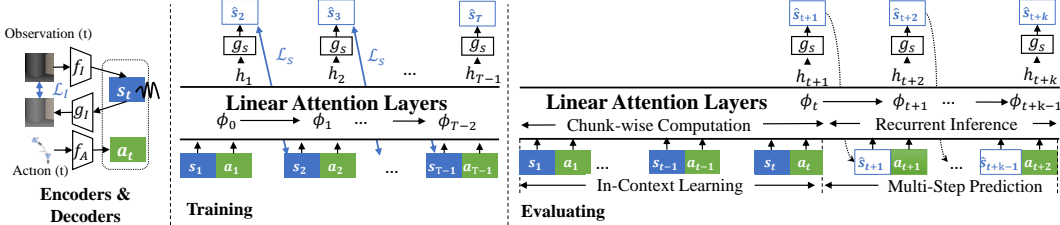


Figure 1: The world model structure for the empirical study.

### 3.4 L2World: Long-Context and Linear-Attention World Models

Prior work relies on multi-token representations or diffusion models to deliver high-fidelity single-frame reconstructions specifically for images. While these approaches set the state-of-the-art for static images, they introduce prohibitive memory and computational bottlenecks when sequences grow to the length required for ICEL. We therefore introduce L2World that trade per-frame fidelity for temporal scalability: for image observations, we compress each frame  $o_t$  into a latent state  $s_t$  with a lightweight variational auto-encoder (VAE) [66] whose encoder  $f_I$  and decoder  $g_I$  are ResNet stacks; for low-dimensional observations, we simply apply a small multi-layer perceptron encoder/decoder pair. For computational efficiency, we do not model the full state estimation with  $\hat{p}(s_t|q_t)$ . Instead, we construct a pseudo-state that depends solely on the instant observation and leaves all temporal-related encoding to transition modeling [4]. We then construct the adaptive world model  $\hat{p}_\theta(o_{t+1}|q_t, C_T)$  using an efficient sequence decoder  $f_\theta$ . Here we implement gated slot attention layers [67–69] with chunk-wise parallelization during the training phase, while retaining the recurrent form during the inference phase. The predictor of transition at first yields the output  $h_t$ , which is further processed by the decoder  $g_S$  to produce the predicted state  $\hat{s}$ , corresponding to predicting a Gaussian distribution over the latent space  $\hat{p} \sim \mathcal{N}(\hat{s}_t, \sigma_s^2)$ . Although this assumption could lead to significant loss of accuracy in stochastic environments, for the navigation tasks we consider, it is acceptable and greatly increases computational efficiency. The model and the target function are listed as follows (see details in Section B.2):

$$\begin{aligned}
 &\text{Observation Encoder : } s_t, \sigma_{s,t} = f_I(o_t) && \text{Observation Decoder : } \hat{o}_t = g_I(\hat{s}_t) \\
 &\text{Latent Decoder : } \hat{s}_t, \hat{\sigma}_{s,t} = g_S(h_t) && \text{Action Encoder : } a_t = f_A(\text{Action}[t]) \\
 &\text{Chunk-wise Temporal Modeling : } \phi_t, h_1, \dots, h_t = f_\theta(s_1, a_1, \dots, s_t, a_t) \\
 &\text{Recurrent Temporal Modeling (Evaluating) : } \phi_t, h_{t+1} = f_\theta(\phi_{t-1}, s_t, a_t) \\
 &\text{Observation Reconstruction Loss : } \mathcal{L}_o = \|o_t - g_I(\hat{s}_t)\| + \lambda KL(\mathcal{N}(s_t, \sigma_{s,t}) \| \mathcal{N}(0, 1)) \\
 &\text{State Transition Loss : } \mathcal{L}_s = - \sum_t KL(\mathcal{N}(s_t, \sigma_{s,t}) \| \mathcal{N}(\hat{s}_t, \hat{\sigma}_{s,t}))
 \end{aligned}$$

When the observation is an image, we first pre-train the image encoder  $f_O$  and decoder  $g_O$  on pre-sampled observations; after this stage, their parameters are frozen while the temporal model is trained. For lower-dimensional observations, all encoders/decoders are updated jointly with the temporal model in a single end-to-end phase.

## 4 Experiments

Although prior studies [62, 65, 53] have validated the influence of data distribution on ICL, they have largely concentrated on simplified tasks such as regression and classification. To examine how data distribution, model architecture, and training procedure jointly affect the emergence of ICEL/ICER,

we select two canonical benchmarks. First, the cart-pole, a classical continuous-control problem, in which ICEL primarily targets the acquisition of varying embodiments and physical constants. Second, indoor navigation, a widely recognized POMDP, in which ICEL focuses on learning and memorizing spatial coefficients. These two experiments confirm not only the impact of each factor on ICEL but also demonstrate that ICEL spans a broad generalization spectrum, extending from spatial reasoning and memorization to adaptation of embodiment and physical constants.

#### 4.1 Random Cart-Poles

**Experiment Setting.** To investigate ICEL and ICER in cart-pole environments, we randomized four variables in the environment settings: gravity  $g$ , cart mass  $m_c$ , pole mass  $m_p$ , and pole length  $l$ . We focus on two different scopes of the configurations to investigate the impact of the diversity issue: Scope 1 remains close to the original task, whereas Scope 2 covers a larger region and excludes Scope 1 (details are left to Figure 5). For each environment, we first trained an RL agent and then collected trajectories with an expert policy perturbed by uniform noise spanning  $[0.3, 0.7]$  to ensure adequate coverage of the state-action space. We trained five comparison models; all share the same data scale (128K trajectories  $\times$  200 step/trajectory) but differ in the number and scope of the environments.

- 1-Env: 96K trajectories are sampled from the original environment ( $g = 9.8, m_c = 1.0, m_p = 0.1, l = 0.5$ ), with 200 steps per trajectory.
- 4-Envs: 4 environments sampled from Scope 1+2, each with 24K trajectories.
- 16-Envs: 16 environments sampled from Scope 1+2, each with 8K trajectories.
- 8K-Envs (Scope 1/1+2): 8,000 environments sampled from Scope 1 or 1+2, each with 16 trajectories.

We evaluate with three test sets: (1) Seen 4-Envs, but the trajectories are independently sampled; (2) 256 environments from Scope 1; and (3) 256 environments from Scope 2. We evaluate mainly with the average prediction error, which is averaged over each of the context lengths  $T$ .

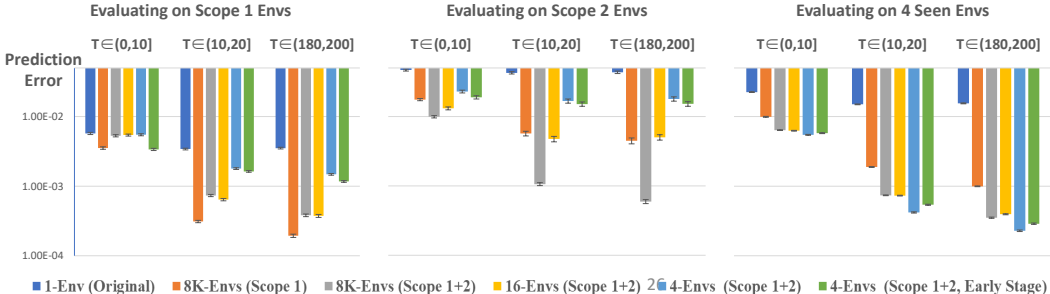


Figure 2: Comparison of models trained on different datasets (color-coded) in Cart-Poles. Performance varies markedly with the training data, revealing distinct tendencies toward ICER, ICEL, or an inability to perform ICL.

We plot the evaluation results in Figure 2, where the following insight is worth noting:

**Importance of both environment scope and environment number:** A comparison between the model trained on 1 environment (1 Env) and 4 environments (4 Envs) with the other group demonstrates that an insufficient number of environments leads to the absence of ICL and generalization, except in the tasks that the model has already seen. The 4 Envs group exhibits clear ICER characteristics, with a substantial performance gap between seen and unseen tasks. The 16 Envs (Scope 1 + 2) and 8K Envs (Scope 1) groups display similar capabilities; however, they lag significantly behind the 8K Envs (Scope 1 + 2) group, indicating that both the scope of tasks and the number of tasks are crucial.

**Divergence between few-shot and many-shot performances:** Another insight gleaned from the comparison between 4-Envs and 8K-Envs is that the latter, which has a broader generalization scope, also requires more context to learn. This is evidenced by the fact that the performance of the latter group does not surpass that of the former group until  $T > 10$ . This also validates the theoretical analysis, indicating that a longer context is a cost for achieving better generalization.

Table 1: A summary of data distribution across the training datasets.

Training DataSet	# envs ( $ \mathcal{E} $ )	Len. Traj.	# Traj.	# frames	Indoor area
Maze-32K-L	32K	10K	32K	320M	$380 \sim 3422m^2$
Maze-32K-S	32K	100	3.2M	320M	$380 \sim 3422m^2$
Maze-128-L	128	10K	32K	320M	$380 \sim 3422m^2$
Maze-128-S	128	100	3.2M	320M	$380 \sim 3422m^2$
ProcTHOR-5K	5K	2K	5K	10M	$40 \sim 600m^2$
ProcTHOR-40K	40K	2K	40K	80M	$40 \sim 600m^2$

**Over-training reduces generalization when training environments are insufficient:** To isolate the effect of over-training, we extract an early-stage checkpoint from the 4-Env group and evaluate it across all environments. Although its performance in seen environments is sub-optimal, it generalizes to unseen environments with a considerable margin over the over-trained model, confirming the shift from ICL- to IWL-based reliance.

## 4.2 Navigation

**Experiment settings.** Procedurally generated mazes are a demanding test-bed for transition prediction [70, 71]. By stripping observations of semantic cues, the maze framework keeps task complexity low while still exposing models to stochastic, partially observable dynamics. We amplify diversity through fully randomized configurations that vary topology, textures, object placement, and agent embodiment <sup>1</sup>. Room-tour data are collected in a way similar to cart-pole: we perturb the oracle object-navigation policy [72, 70] with random noise levels in  $[0.05, 0.95]$  and record the complete trajectory of an agent in each environment. The oracle policy was derived using Dijkstra’s algorithm based on the ground truth 2-D occupancy maps. Observations are RGB images standardized to  $128 \times 128$  pixels; The action space comprises 17 discrete actions, each corresponding to a unique offset and rotational movement. Table 1 lists the resulting training sets, each drawn from a different number of environments and exhibiting varying trajectory lengths. To isolate the effect of data distribution, all maze datasets contain the same number of frames while differing in the coverage of trajectories and environments. To further investigate its transferability to more realistic environments, we also collect trajectories from the semantically rich ProcTHOR simulation, which offers a wide variety of assets [73, 74]. Specifically, we curate two datasets: a larger one with 40K trajectories and a smaller one with 5K trajectories, each trajectory having a length of 2K.

For training, inspired by overshooting [43] and Hu et al. [38], we randomly mask the  $s_t$  of the input sequences at some positions to enhance the model’s capability to predict the distant future (see training details in Section B.1). Evaluation is conducted on both seen and unseen tasks. By default, we use an evaluation set scale of  $|\mathcal{E}| = 256$ . The evaluation process involves encoding a context of length  $t$  for ICEL and then predicting future  $k$ -step transitions using auto-regression and the ground truth action records  $a_{t+1}, a_{t+2}, \dots, a_{t+k}$ . We assess the error in both the latent spaces and the decoded images, which we refer to as  $k$ -step prediction with context length  $T = t$ . For example,  $T = 10$  and  $k = 4$  predict future 4 steps with a context length of 10.

We evaluate two additional baselines alongside the proposed long-context world model: (1) Navigation World Model (NWM) [7], which employs diffusion layers to predict the next frame from the preceding four frames; (2) Dreamer-v3 [34], which uses LSTM layers for temporal encoding. For NWM, we retain its original pre-trained image encoders and re-train only the diffusion layers on the target dataset. For Dreamer-v3, we remove the policy components and train only the world-model module to ensure a fair comparison.

**Impact of data distribution and model architecture on ICEL.** Table 2 reports the next-frame prediction quality estimated by PSNR ( $k = 1$ ) for models trained on different datasets. Three empirical findings corroborate Theorem 1: (1) The 32K-L dataset yields the best generalization to unseen environments, whereas the 128-L dataset excels on seen ones; in both cases, peak performance occurs at the asymptotic stage, not at the beginning of the context. (2) Long-context training consistently produces stronger ICL than short-context training, confirming that extensive context is necessary for ICL to emerge. (3) Dreamer and NWM fall short even with a long-context dataset:

<sup>1</sup>Procedural Maze environments:

<https://github.com/FutureAGI/Xenoverse/tree/main/xenoverse/mazeworld>

Table 2: Comparison of the performances (PSNR  $\uparrow$ ) of 1-step future prediction in Mazes.

Model	Seen					Unseen				
	T=1	T=10	T=100	T=1000	T=10000	T=1	T=10	T=100	T=1000	T=10000
L2World (Maze-32K-L)	16.80	20.97	23.11	24.65	25.05	16.37	<b>21.24</b>	<b>23.17</b>	<b>24.66</b>	<b>24.65</b>
L2World (Maze-32K-S)	18.57	19.28	19.67	20.21	20.48	<b>18.45</b>	19.24	19.63	20.29	20.31
L2World (Maze-128-S)	19.47	20.39	20.58	22.02	21.77	18.01	18.63	19.00	19.67	19.63
L2World (Maze-128-L)	18.54	20.86	<b>23.32</b>	<b>25.65</b>	<b>26.00</b>	17.54	19.43	20.96	21.54	21.52
Dreamer (Maze-32K-L)	16.40	<b>21.82</b>	19.24	21.26	21.89	16.81	20.48	21.40	22.65	22.12
Dreamer (Maze-128-L)	17.13	20.64	21.83	22.20	22.43	14.26	14.54	14.09	13.46	13.50
NWM (Maze-32K-L)	<b>20.84</b>	20.21	19.19	22.32	21.06	16.20	16.71	17.00	17.37	17.85

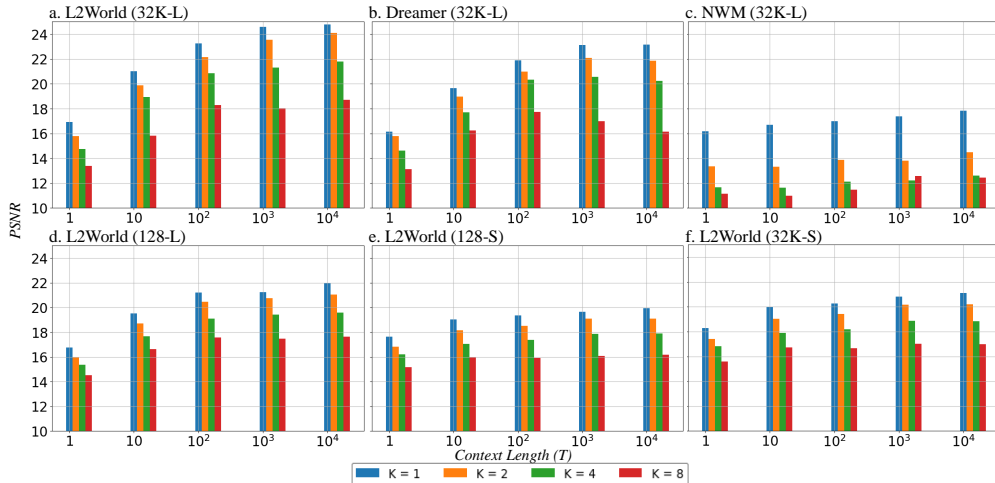


Figure 3: Comparison of  $k$ -step autoregressive PSNR in Mazes(Unseen).

Dreamer’s LSTM backbone and NWM’s 4-frame horizon show that architectures incapable of fully leveraging long contexts cannot achieve many-shot ICEL. Figure 3 further presents the  $k = \{1, 2, 4, 8\}$ -step prediction performances on unseen Mazes, measuring how far ahead the world models can reliably foresee. For  $k > 1$ , the performance–context-length curve largely tracks the next-frame trend across models, except for Dreamer (Maze 32K-L): at  $k = 8$ , its performance plateaus once  $T > 100$ , whereas  $k = 1$  keeps improving, revealing a larger compound-error accumulation than in our method.

Figure 4 illustrates 10-step-ahead predictions at  $T = \{1, 100, 10K\}$  for our method, Dreamer, and NWM trained on Maze-32K-L. NWM produces visually convincing frames with fine textures and a plausible layout, yet frame-wise fidelity alone is insufficient for correct long-range forecasting because the model lacks long-term memory and spatial reasoning.

Table 3: Comparison of the PSNR of 1-step future prediction in ProcTHOR (Unseen)

Model	Pre-train	Post-train	T=1	T=10	T=100	T=1000	T=10000
L2World	-	ProcTHOR-5K	15.49	18.22	19.02	19.74	19.81
L2World	Maze-32K-L		16.46	<b>20.23</b>	<b>21.05</b>	<b>21.89</b>	<b>22.04</b>
L2World	Maze-32K-S		<b>19.80</b>	19.45	19.86	20.57	20.61
L2World	Maze-128-L		19.16	19.60	20.20	20.94	16.46
Dreamer	-	ProcTHOR-40K	19.82	22.61	23.99	23.51	22.76
NWM	-		18.30	21.41	21.11	21.02	20.08
L2World	-		<b>21.57</b>	22.67	23.39	24.92	22.98
L2World	Maze-32K-L		17.21	<b>22.81</b>	<b>24.32</b>	<b>25.40</b>	<b>23.94</b>

**Transferability of ICEL and ICER:** To verify whether ICEL emerges in semantically richer, realistic environments and whether skills acquired in simpler environments transfer to more complex ones, we fine-tune the models on ProcTHOR trajectories and evaluate them in varied contexts, as shown in Table 3. The model pre-trained on Maze-32K-L not only excels in unseen mazes but also retains its advantage when fine-tuned on the small ProcTHOR-5K set; its transferability markedly exceeds that of Maze-128-L and other baselines, evidencing ICEL’s domain-generality. Further increasing

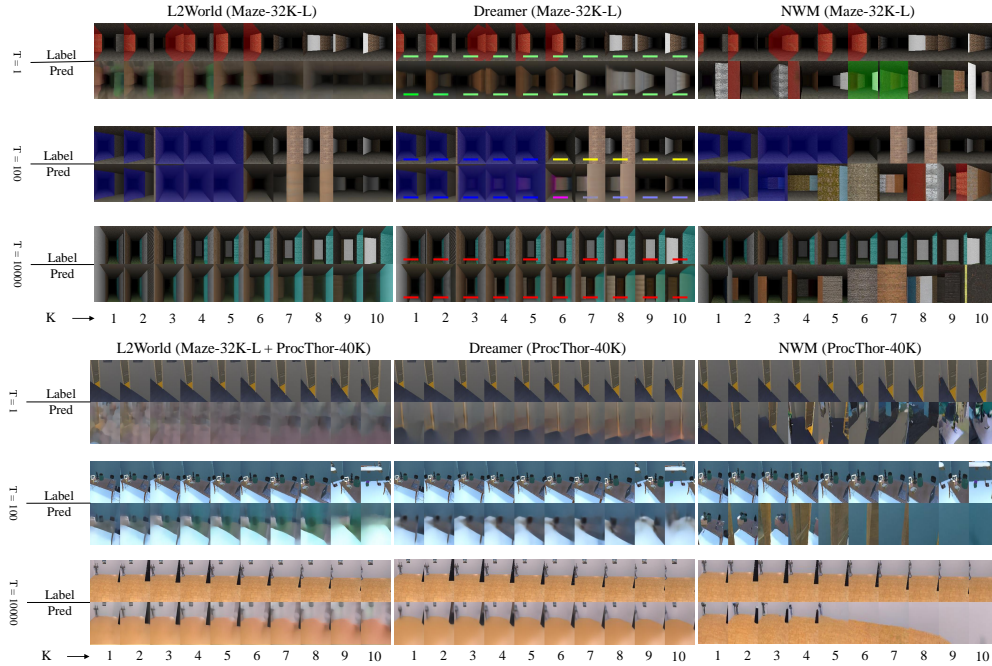


Figure 4: Example predictions produced by L2World and the baselines in Mazes and ProcTHOR for  $T = \{1, 100, 10000\}$  and  $k = 10$ , together with the corresponding ground-truth sequences.

ProcTHOR data yields continual improvement in our model while maintaining a large margin over Dreamer and NWM. However, the performance from  $T = 1K$  to  $T = 10K$  begins to deteriorate once the training data switches from ProcTHOR-5K to ProcTHOR-40K, implying that ProcTHOR trajectories with  $T \leq 2K$  fail to incentivize ICeL at longer contexts. Yet, this phenomenon does not appear with ProcTHOR-5K, verifying that the ICeL capability acquired in L2World transfers effectively to ProcTHOR despite the large gap between the two classes of environments.

## 5 Conclusions and Limitations

**Conclusions:** This work investigates in-context learning of world models, specifically dynamic models, focusing on the possible modes of ICeL and ICeR in MDP and POMDP. Theoretically, we analyze error upper bounds for both modes to characterize their properties and identify the conditions under which each excels. Empirically, we introduce L2World and validate these insights in cart-pole and navigation tasks. Our results underscore that both high environment diversity and sufficient context length of the world model are essential to elicit ICeL.

**Limitations:** At present, our analysis is confined to the dynamic model; the reward and policy models can be addressed subsequently. This work constitutes a first step toward broader ICL mechanisms such as In-Context Reinforcement Learning. More sophisticated validations on real-world datasets and environments are desirable in the future.

## Acknowledgments and Disclosure of Funding

This project is supported by Longgang District Shenzhen’s “Ten Action Plan” for supporting innovation projects (under Grant LGKCSPT2024002).

## References

- [1] David R Ha and Jürgen Schmidhuber. World models. *ArXiv*, abs/1803.10122, 2018. URL <https://api.semanticscholar.org/CorpusID:4807711>.
- [2] Danijar Hafner, Jurgis Pasukonis, Jimmy Ba, and Timothy Lillicrap. Mastering diverse control tasks through world models. *Nature*, pages 1–7, 2025.
- [3] Weipu Zhang, Gang Wang, Jian Sun, Yetian Yuan, and Gao Huang. Storm: Efficient stochastic transformer based world models for reinforcement learning. *Advances in Neural Information Processing Systems*, 36:27147–27166, 2023.
- [4] Pietro Mazzaglia, Tim Verbelen, Bart Dhoedt, Aaron Courville, and Sai Rajeswar. Genrl: Multimodal-foundation world models for generalization in embodied agents. *Advances in Neural Information Processing Systems*, 37:27529–27555, 2024.
- [5] Mohammad Reza Samsami, Artem Zholus, Janarthanan Rajendran, and Sarath Chandar. Mastering memory tasks with world models. In *The Twelfth International Conference on Learning Representations*, 2024.
- [6] Eloi Alonso, Adam Jelley, Vincent Micheli, Anssi Kanervisto, Amos J Storkey, Tim Pearce, and François Fleuret. Diffusion for world modeling: Visual details matter in atari. *Advances in Neural Information Processing Systems*, 37:58757–58791, 2024.
- [7] Amir Bar, Gaoyue Zhou, Danny Tran, Trevor Darrell, and Yann LeCun. Navigation world models. In *Proceedings of the Computer Vision and Pattern Recognition Conference (CVPR)*, pages 15791–15801, June 2025.
- [8] Russell Mendonca, Oleh Rybkin, Kostas Daniilidis, Danijar Hafner, and Deepak Pathak. Discovering and achieving goals via world models. In M. Ranzato, A. Beygelzimer, Y. Dauphin, P.S. Liang, and J. Wortman Vaughan, editors, *Advances in Neural Information Processing Systems*, volume 34, pages 24379–24391. Curran Associates, Inc., 2021. URL [https://proceedings.neurips.cc/paper\\_files/paper/2021/file/cc4af25fa9d2d5c953496579b75f6f6c-Paper.pdf](https://proceedings.neurips.cc/paper_files/paper/2021/file/cc4af25fa9d2d5c953496579b75f6f6c-Paper.pdf).
- [9] Jing Yu Koh, Honglak Lee, Yinfei Yang, Jason Baldridge, and Peter Anderson. Pathdreamer: A world model for indoor navigation. In *Proceedings of the IEEE/CVF International Conference on Computer Vision*, pages 14738–14748, 2021.
- [10] Yuanlin Duan, Wensen Mao, and He Zhu. Learning world models for unconstrained goal navigation. In *The Thirty-eighth Annual Conference on Neural Information Processing Systems*, 2024. URL <https://openreview.net/forum?id=aYqTwcDlCG>.
- [11] Zeyuan Liu, Ziyu Huan, Xiyao Wang, Jiafei Lyu, Jian Tao, Xiu Li, Furong Huang, and Huazhe Xu. World models with hints of large language models for goal achieving. In Luis Chiruzzo, Alan Ritter, and Lu Wang, editors, *Proceedings of the 2025 Conference of the Nations of the Americas Chapter of the Association for Computational Linguistics: Human Language Technologies (Volume 1: Long Papers)*, pages 50–72, Albuquerque, New Mexico, April 2025. Association for Computational Linguistics. ISBN 979-8-89176-189-6. URL <https://aclanthology.org/2025.naacl-long.3/>.
- [12] Anthony Hu, Lloyd Russell, Hudson Yeo, Zak Murez, George Fedoseev, Alex Kendall, Jamie Shotton, and Gianluca Corrado. Gaia-1: A generative world model for autonomous driving. *ArXiv*, abs/2309.17080, 2023. URL <https://api.semanticscholar.org/CorpusID:263310665>.

- [13] Lloyd Russell, Anthony Hu, Lorenzo Bertoni, George Fedoseev, Jamie Shotton, Elahe Arani, and Gianluca Corrado. Gaia-2: A controllable multi-view generative world model for autonomous driving. *arXiv preprint arXiv:2503.20523*, 2025.
- [14] Shenyuan Gao, Jiazhi Yang, Li Chen, Kashyap Chitta, Yihang Qiu, Andreas Geiger, Jun Zhang, and Hongyang Li. Vista: A generalizable driving world model with high fidelity and versatile controllability. In A. Globerson, L. Mackey, D. Belgrave, A. Fan, U. Paquet, J. Tomczak, and C. Zhang, editors, *Advances in Neural Information Processing Systems*, volume 37, pages 91560–91596. Curran Associates, Inc., 2024. URL [https://proceedings.neurips.cc/paper\\_files/paper/2024/file/a6a066fb44f2fe0d36cf740c873b8890-Paper-Conference.pdf](https://proceedings.neurips.cc/paper_files/paper/2024/file/a6a066fb44f2fe0d36cf740c873b8890-Paper-Conference.pdf).
- [15] Lunjun Zhang, Yuwen Xiong, Ze Yang, Sergio Casas, Rui Hu, and Raquel Urtasun. Copilot4d: Learning unsupervised world models for autonomous driving via discrete diffusion. In *The Twelfth International Conference on Learning Representations*, 2024. URL <https://openreview.net/forum?id=Ps175UCoZM>.
- [16] Yuqi Wang, Jiawei He, Lue Fan, Hongxin Li, Yuntao Chen, and Zhaoxiang Zhang. Driving into the future: Multiview visual forecasting and planning with world model for autonomous driving. In *Proceedings of the IEEE/CVF Conference on Computer Vision and Pattern Recognition*, pages 14749–14759, 2024.
- [17] Zhejun Zhang, Alexander Liniger, Dengxin Dai, Fisher Yu, and Luc Van Gool. Trafficbots: Towards world models for autonomous driving simulation and motion prediction. In *2023 IEEE International Conference on Robotics and Automation (ICRA)*, pages 1522–1529, 2023. doi: 10.1109/ICRA48891.2023.10161243.
- [18] Philipp Wu, Alejandro Escontrela, Danijar Hafner, Pieter Abbeel, and Ken Goldberg. Daydreamer: World models for physical robot learning. In *Conference on robot learning*, pages 2226–2240. PMLR, 2023.
- [19] Nicklas Hansen, Hao Su, and Xiaolong Wang. TD-MPC2: Scalable, robust world models for continuous control. In *The Twelfth International Conference on Learning Representations*, 2024. URL <https://openreview.net/forum?id=0xh5CstDJU>.
- [20] Jing-Cheng Pang, Nan Tang, Kaiyuan Li, Yuting Tang, Xin-Qiang Cai, Zhen-Yu Zhang, Gang Niu, Masashi Sugiyama, and Yang Yu. Learning view-invariant world models for visual robotic manipulation. In *The Thirteenth International Conference on Learning Representations*, 2025. URL <https://openreview.net/forum?id=vJwjWyt4Ed>.
- [21] Siyuan Zhou, Yilun Du, Jiaben Chen, Yandong Li, Dit-Yan Yeung, and Chuang Gan. Robodreamer: learning compositional world models for robot imagination. *ICML’24. JMLR.org*, 2024.
- [22] Leonardo Barcellona, Andrii Zadaianchuk, Davide Allegro, Samuele Papa, Stefano Ghidoni, and Efstratios Gavves. Dream to manipulate: Compositional world models empowering robot imitation learning with imagination. In *The Thirteenth International Conference on Learning Representations*, 2025. URL <https://openreview.net/forum?id=3RSLW9YSgk>.
- [23] Charles V Vorhees and Michael T Williams. Assessing spatial learning and memory in rodents. *ILAR journal*, 55(2):310–332, 2014.
- [24] Rajesh PN Rao and Dana H Ballard. Predictive coding in the visual cortex: a functional interpretation of some extra-classical receptive-field effects. *Nature neuroscience*, 2(1):79–87, 1999.
- [25] Tommaso Salvatori, Ankur Mali, Christopher L Buckley, Thomas Lukasiewicz, Rajesh PN Rao, Karl Friston, and Alexander Ororbia. A survey on brain-inspired deep learning via predictive coding. *arXiv preprint arXiv:2308.07870*, 2023.
- [26] Tom Brown, Benjamin Mann, Nick Ryder, Melanie Subbiah, Jared D Kaplan, Prafulla Dhariwal, Arvind Neelakantan, Pranav Shyam, Girish Sastry, Amanda Askell, et al. Language models are few-shot learners. *Advances in neural information processing systems*, 33:1877–1901, 2020.

- [27] Jay Wright Forrester. Industrial dynamics. *Harvard Business Review*, 36(4):37–66, 1958.
- [28] Richard S Sutton. Integrated architectures for learning, planning, and reacting based on approximating dynamic programming. In *Machine learning proceedings 1990*, pages 216–224. Elsevier, 1990.
- [29] Peter W Battaglia, Jessica B Hamrick, and Joshua B Tenenbaum. Simulation as an engine of physical scene understanding. *Proceedings of the National Academy of Sciences*, 110(45):18327–18332, 2013.
- [30] David Ha and Jürgen Schmidhuber. Recurrent world models facilitate policy evolution. *Advances in neural information processing systems*, 31, 2018.
- [31] Yann LeCun. A path towards autonomous machine intelligence. *Open Review*, 2022.
- [32] Chelsea Finn and Sergey Levine. Deep visual foresight for planning robot motion. In *2017 IEEE International Conference on Robotics and Automation (ICRA)*, pages 2786–2793, 2017.
- [33] Julian Schrittwieser, Ioannis Antonoglou, Thomas Hubert, Karen Simonyan, Laurent Sifre, Simon Schmitt, Arthur Guez, Edward Lockhart, Demis Hassabis, Thore Graepel, et al. Mastering atari, go, chess and shogi by planning with a learned model. *Nature*, 588(7839):604–609, 2020.
- [34] Danijar Hafner, Timothy Lillicrap, Jimmy Ba, et al. Dream to control: Learning behaviors by latent imagination. *arXiv preprint arXiv:1912.01603*, 2019.
- [35] Richard S Sutton. Dyna, an integrated architecture for learning, planning, and reacting based on approximating dynamic programming. *ACM Sigart Bulletin*, 2(4):160–163, 1991.
- [36] Łukasz Kaiser, Mohammad Babaeizadeh, Piotr Miłoś, Błażej Osipiński, Roy H Campbell, Konrad Czechowski, Dumitru Erhan, Chelsea Finn, Piotr Kozakowski, Sergey Levine, et al. Model based reinforcement learning for atari. In *International Conference on Learning Representations*, 2020.
- [37] Max Jaderberg, Volodymyr Mnih, Wojciech Marian Czarnecki, Tom Schaul, Joel Z Leibo, David Silver, and Koray Kavukcuoglu. Reinforcement learning with unsupervised auxiliary tasks. *arXiv preprint arXiv:1611.05397*, 2016.
- [38] Anthony Hu, Gianluca Corrado, Nicolas Griffiths, Zak Murez, Corina Gurau, Hudson Yeo, Alex Kendall, Roberto Cipolla, and Jamie Shotton. Model-based imitation learning for urban driving. In *Proceedings of the 36th International Conference on Neural Information Processing Systems, NIPS ’22*, Red Hook, NY, USA, 2022. Curran Associates Inc. ISBN 9781713871088.
- [39] Yumeng Zhang, Shi Gong, Kaixin Xiong, Xiaoqing Ye, Xiao Tan, Fan Wang, Jizhou Huang, Hua Wu, and Haifeng Wang. Bevworld: A multimodal world model for autonomous driving via unified bev latent space. *arXiv preprint arXiv:2407.05679*, 2024.
- [40] Ian Goodfellow, Jean Pouget-Abadie, Mehdi Mirza, et al. Generative adversarial nets. In *Advances in Neural Information Processing Systems*, pages 2672–2680, 2014.
- [41] Diederik P Kingma and Max Welling. Auto-encoding variational bayes. *arXiv preprint arXiv:1312.6114*, 2013.
- [42] ZiRui Wang, Yue Deng, Junfeng Long, and Yin Zhang. Parallelizing model-based reinforcement learning over the sequence length. *Advances in Neural Information Processing Systems*, 37:131398–131433, 2024.
- [43] Danijar Hafner, Timothy Lillicrap, Ian Fischer, Ruben Villegas, David Ha, Honglak Lee, and James Davidson. Learning latent dynamics for planning from pixels. In *International conference on machine learning*, pages 2555–2565. PMLR, 2019.
- [44] Quentin Garrido, Mahmoud Assran, Nicolas Ballas, Adrien Bardes, Laurent Najman, and Yann LeCun. Learning and leveraging world models in visual representation learning. *arXiv preprint arXiv:2403.00504*, 2024.

- [45] Yingyan Li, Lue Fan, Jiawei He, Yuqi Wang, Yuntao Chen, Zhaoxiang Zhang, and Tieniu Tan. Enhancing end-to-end autonomous driving with latent world model. *arXiv preprint arXiv:2406.08481*, 2024.
- [46] Rudra P. K. Poudel, Harit Pandya, Chao Zhang, and Roberto Cipolla. Langwm: Language grounded world model. *ArXiv*, abs/2311.17593, 2023. URL <https://api.semanticscholar.org/CorpusID:265498747>.
- [47] Dujun Nie, Xianda Guo, Yiqun Duan, Ruijun Zhang, and Long Chen. Wmnav: Integrating vision-language models into world models for object goal navigation, 2025. URL <https://arxiv.org/abs/2503.02247>.
- [48] Rui Liu, Xiaohan Wang, Wenguan Wang, and Yi Yang. Bird’s-eye-view scene graph for vision-language navigation. In *Proceedings of the IEEE/CVF International Conference on Computer Vision*, pages 10968–10980, 2023.
- [49] Shibhansh Dohare, J Fernando Hernandez-Garcia, Qingfeng Lan, Parash Rahman, A Rupam Mahmood, and Richard S Sutton. Loss of plasticity in deep continual learning. *Nature*, 632(8026):768–774, 2024.
- [50] Adam Santoro, Sergey Bartunov, Matthew Botvinick, Daan Wierstra, and Timothy Lillicrap. Meta-learning with memory-augmented neural networks. In *International conference on machine learning*, pages 1842–1850. PMLR, 2016.
- [51] Yan Duan, John Schulman, Xi Chen, Peter L Bartlett, Ilya Sutskever, and Pieter Abbeel.  $RI^2$ : Fast reinforcement learning via slow reinforcement learning. *arXiv preprint arXiv:1611.02779*, 2016.
- [52] Ekin Akyürek, Bailin Wang, Yoon Kim, and Jacob Andreas. In-context language learning: architectures and algorithms. In *Proceedings of the 41st International Conference on Machine Learning*, pages 787–812, 2024.
- [53] Allan Raventós, Mansheej Paul, Feng Chen, and Surya Ganguli. Pretraining task diversity and the emergence of non-bayesian in-context learning for regression. *Advances in neural information processing systems*, 36:14228–14246, 2023.
- [54] Sang Michael Xie, Aditi Raghunathan, Percy Liang, and Tengyu Ma. An explanation of in-context learning as implicit bayesian inference. In *International Conference on Learning Representations*, 2024.
- [55] Michael Laskin, Luyu Wang, Junhyuk Oh, Emilio Parisotto, Stephen Spencer, Richie Steigerwald, DJ Strouse, Steven Stenberg Hansen, Angelos Filos, Ethan Brooks, et al. In-context reinforcement learning with algorithm distillation. In *The Eleventh International Conference on Learning Representations*, 2023.
- [56] Jonathan Lee, Annie Xie, Aldo Pacchiano, Yash Chandak, Chelsea Finn, Ofir Nachum, and Emma Brunskill. Supervised pretraining can learn in-context reinforcement learning. *Advances in Neural Information Processing Systems*, 36:43057–43083, 2023.
- [57] Fan Wang, Pengtao Shao, Yiming Zhang, Bo Yu, Shaoshan Liu, Ning Ding, Yang Cao, Yu Kang, and Haifeng Wang. Towards large-scale in-context reinforcement learning by meta-training in randomized worlds, 2025. URL <https://arxiv.org/abs/2502.02869>.
- [58] Ankesh Anand, Jacob C Walker, Yazhe Li, Eszter Vértés, Julian Schrittwieser, Sherjil Ozair, Theophane Weber, and Jessica B Hamrick. Procedural generalization by planning with self-supervised world models. In *International Conference on Learning Representations*, 2022. URL <https://openreview.net/forum?id=FmBegXJToY>.
- [59] Sharut Gupta, Chenyu Wang, Yifei Wang, Tommi Jaakkola, and Stefanie Jegelka. In-context symmetries: Self-supervised learning through contextual world models. In A. Globerson, L. Mackey, D. Belgrave, A. Fan, U. Paquet, J. Tomczak, and C. Zhang, editors, *Advances in Neural Information Processing Systems*, volume 37, pages 104250–104280. Curran Associates, Inc., 2024. URL [https://proceedings.neurips.cc/paper\\_files/paper/2024/file/bcad07d4bfab51243efaa08b8ed475b3-Paper-Conference.pdf](https://proceedings.neurips.cc/paper_files/paper/2024/file/bcad07d4bfab51243efaa08b8ed475b3-Paper-Conference.pdf).

- [60] Gili Lior, Yuval Shalev, Gabriel Stanovsky, and Ariel Goldstein. Computation or weight adaptation? rethinking the role of plasticity in learning. *bioRxiv*, pages 2024–03, 2024.
- [61] Jane Pan, Tianyu Gao, Howard Chen, and Danqi Chen. What in-context learning “learns” in-context: Disentangling task recognition and task learning. In *Findings of the Association for Computational Linguistics, ACL 2023*, Proceedings of the Annual Meeting of the Association for Computational Linguistics, pages 8298–8319. Association for Computational Linguistics (ACL), 2023. doi: 10.18653/v1/2023.findings-acl.527. Publisher Copyright: © 2023 Association for Computational Linguistics.; 61st Annual Meeting of the Association for Computational Linguistics, ACL 2023 ; Conference date: 09-07-2023 Through 14-07-2023.
- [62] Stephanie Chan, Adam Santoro, Andrew Lampinen, Jane Wang, Aaditya Singh, Pierre Richemond, James McClelland, and Felix Hill. Data distributional properties drive emergent in-context learning in transformers. *Advances in neural information processing systems*, 35:18878–18891, 2022.
- [63] Bryan Chan, Xinyi Chen, András György, and Dale Schuurmans. Toward understanding in-context vs. in-weight learning. In *The Thirteenth International Conference on Learning Representations*, 2025. URL <https://openreview.net/forum?id=aKJr5Nn8U>.
- [64] Louis Kirsch, James Harrison, Jascha Sohl-Dickstein, and Luke Metz. General-purpose in-context learning by meta-learning transformers. In *Sixth Workshop on Meta-Learning at the Conference on Neural Information Processing Systems*, 2022.
- [65] Aaditya Singh, Stephanie Chan, Ted Moskovitz, Erin Grant, Andrew Saxe, and Felix Hill. The transient nature of emergent in-context learning in transformers. *Advances in neural information processing systems*, 36:27801–27819, 2023.
- [66] Diederik P Kingma and Max Welling. Auto-encoding variational bayes. In *2nd International Conference on Learning Representations*, 2014.
- [67] Sinong Wang, Belinda Z Li, Madian Khabsa, Han Fang, and Hao Ma. Linformer: Self-attention with linear complexity. *arXiv preprint arXiv:2006.04768*, 2020.
- [68] Songlin Yang, Bailin Wang, Yikang Shen, Rameswar Panda, and Yoon Kim. Gated linear attention transformers with hardware-efficient training. In *International Conference on Machine Learning*, pages 56501–56523. PMLR, 2024.
- [69] Yu Zhang, Songlin Yang, Rui-Jie Zhu, Yue Zhang, Leyang Cui, Yiqiao Wang, Bolun Wang, Freda Shi, Bailin Wang, Wei Bi, et al. Gated slot attention for efficient linear-time sequence modeling. *Advances in Neural Information Processing Systems*, 37:116870–116898, 2024.
- [70] Jurgis Pašukonis, Timothy P Lillicrap, and Danijar Hafner. Evaluating long-term memory in 3d mazes. In *The Eleventh International Conference on Learning Representations*, 2023.
- [71] Fan Wang, Chuan Lin, Yang Cao, and Yu Kang. Benchmarking general-purpose in-context learning. *arXiv preprint arXiv:2405.17234*, 2024.
- [72] Kiana Ehsani, Tanmay Gupta, Rose Hendrix, Jordi Salvador, Luca Weihs, Kuo-Hao Zeng, Kunal Pratap Singh, Yejin Kim, Winson Han, Alvaro Herrasti, et al. Spoc: Imitating shortest paths in simulation enables effective navigation and manipulation in the real world. In *Proceedings of the IEEE/CVF Conference on Computer Vision and Pattern Recognition*, pages 16238–16250, 2024.
- [73] Eric Kolve, Roozbeh Mottaghi, Winson Han, Eli VanderBilt, Luca Weihs, Alvaro Herrasti, Matt Deitke, Kiana Ehsani, Daniel Gordon, Yuke Zhu, et al. Ai2-thor: An interactive 3d environment for visual ai. *arXiv preprint arXiv:1712.05474*, 2017.
- [74] Matt Deitke, Eli VanderBilt, Alvaro Herrasti, Luca Weihs, Kiana Ehsani, Jordi Salvador, Winson Han, Eric Kolve, Aniruddha Kembhavi, and Roozbeh Mottaghi. Procthor: Large-scale embodied ai using procedural generation. *Advances in Neural Information Processing Systems*, 35:5982–5994, 2022.

- [75] Yian Wang, Xiaowen Qiu, Jiageng Liu, Zhehuan Chen, Jiting Cai, Yufei Wang, Tsun-Hsuan Johnson Wang, Zhou Xian, and Chuang Gan. Architect: Generating vivid and interactive 3d scenes with hierarchical 2d inpainting. *Advances in Neural Information Processing Systems*, 37:67575–67603, 2024.
- [76] Adam Paszke, Sam Gross, Francisco Massa, Adam Lerer, James Bradbury, Gregory Chanan, Trevor Killeen, Zeming Lin, Natalia Gimelshein, Luca Antiga, Alban Desmaison, Andreas Köpf, Edward Yang, Zach DeVito, Martin Raison, Alykhan Tejani, Sasank Chilamkurthy, Benoit Steiner, Lu Fang, Junjie Bai, and Soumith Chintala. *PyTorch: an imperative style, high-performance deep learning library*. Curran Associates Inc., Red Hook, NY, USA, 2019.
- [77] Peter J Rousseeuw. Silhouettes: a graphical aid to the interpretation and validation of cluster analysis. *Journal of computational and applied mathematics*, 20:53–65, 1987.

## A Assumptions and Proofs for Theorem 1

**Proof for the first part of Theorem 1:** We first define

$$\begin{aligned}\Delta(e_1, e_2) &= \mathbb{E}_q D_{KL}(\hat{p}_{\theta, e_1}(\cdot|q), \hat{p}_{\theta, e_2}(\cdot|q)) \\ \kappa(e_1, e_2) &= \max_q D_{KL}(\hat{p}_{\theta, e_1}(\cdot|q), \hat{p}_{\theta, e_2}(\cdot|q)) \\ \hat{e}_0 &= \operatorname{argmin}_{e \in \mathcal{E}} \Delta(e, e_0) \\ \kappa_i &= \inf_{e \in \mathcal{E}, e \neq \hat{e}_0} \kappa(e, \hat{e}_0) \\ \kappa_s &= \sup_{e \in \mathcal{E}, e \neq \hat{e}_0} \kappa(e, \hat{e}_0) \\ p_e(C_T) &= \prod_{(q_t, o_{t+1}) \in C_T} p_e(o_{t+1}|q_t)\end{aligned}$$

We then make the following **Assumptions**:

- Queries  $q_t = (s_t, a_t)$  are sampled i.i.d. from a distribution  $\mu(s, a)$  with  $\mu(s, a) \equiv \frac{1}{|S||A|}$ .
- $\kappa(e_1, e_2) = \alpha(e_1, e_2)^2 \Delta(e_1, e_2)$  with  $\alpha(e_1, e_2) = \sqrt{\frac{\kappa(e_1, e_2)}{\Delta(e_1, e_2)}}$ ,  $\alpha > 1$ . We further define  $\alpha = \max_{e_1, e_2} \alpha(e_1, e_2)$ , so that  $\Delta(e_1, e_2) \geq \frac{\kappa(e_1, e_2)}{\alpha^2}$ . Note that  $\alpha$  can be interpreted as the measure of "non-uniformity" between any two environments in the set: it attains maximum when the two environments are almost identical yet differ significantly at only a few positions, and approaches 1 when the environments are either completely different or exactly the same.
- The environment recognizer selects closest task  $\hat{e}$  by  $\hat{e} = \operatorname{argmax}_{e \in \mathcal{E}} p_e(C_T)$

First, we gave that

$$\begin{aligned}TV(\hat{p}_{ER}, p_{e_0}) &= TV(\hat{p}_{\theta, \hat{e}}, p_{e_0}) \leq TV(\hat{p}_{\theta, \hat{e}}, \hat{p}_{\theta, \hat{e}_0}) + TV(\hat{p}_{\theta, \hat{e}_0}, p_{e_0}) \\ &= TV(\hat{p}_{\theta, \hat{e}}, \hat{p}_{\theta, \hat{e}_0}) + \min_{e \in \mathcal{E}} TV(\hat{p}_{\theta, e}, p_{e_0})\end{aligned}$$

We then estimate the first term and use the Chernoff bound for derivation:

$$\begin{aligned}TV(\hat{p}_{\theta, \hat{e}}, \hat{p}_{\theta, \hat{e}_0}) &= \sum_{e \in \mathcal{E}, e \neq \hat{e}_0} p(p_e(C_T) > p_{\hat{e}_0}(C_T)) TV(\hat{p}_{\theta, e}, \hat{p}_{\theta, \hat{e}_0}) \\ &\leq \sum_{e \in \mathcal{E}, e \neq \hat{e}_0} \underbrace{\alpha \cdot \exp(-T \cdot \Delta(e, \hat{e}_0))}_{\text{Chernoff bound}} \underbrace{\sqrt{1/2\Delta(e, \hat{e}_0)}}_{\text{Pinsker's Inequality}} \\ &< \sum_{e \in \mathcal{E}, e \neq \hat{e}_0} \underbrace{\frac{\alpha}{2\sqrt{e \cdot T}}}_{\text{achieved maximum when } T \cdot \Delta(e, \hat{e}_0) = 1/2} \\ &< \frac{\alpha(|\mathcal{E}| - 1)}{3\sqrt{T}}\end{aligned}$$

**Proof for the second part of Theorem 1.** We keep the aforementioned assumptions that the distribution of the context  $C_T$  is uniform on the state and action space. We denote  $n(s, a)$  as times of appearance of  $(s, a)$  in  $C_T$ . It is first straightforward to prove with Hoeffding’s inequality that with probability of  $1 - \delta/2$ ,

$$\frac{T}{|S||A|} - \sqrt{\frac{T \log(4|S||A|/\delta)}{2}} \leq n(s, a \in C_T) \leq \frac{T}{|S||A|} + \sqrt{\frac{T \log(4|S||A|/\delta)}{2}} \quad \forall s, a$$

Then, by add the constraint  $T > 4|S|^2|A|^2 \log(4|S||A|/\delta)$ , with at least probability of  $1 - \delta/2$ ,

$$n(s, a) > \frac{T}{2|S||A|} \tag{6}$$

To estimate  $\hat{p}_{EL}(s'|s, a)$ , we use Equation (4) to acquire:

$$\begin{aligned} \hat{p}_{\theta, EL}(o_{t+1}|q_t, C_T) &= \frac{p(q_t, o_{t+1}|C_T)}{p(q_t|C_T)} \\ &= \frac{\sum_s p(s, a_t, o_{t+1}|C_T)p(s|q_t)}{\sum_s p(s, a_t|C_T)p(s|q_t)} \end{aligned} \tag{7}$$

Now employ Equation (6) and Equation (7) in the calculation of TV:

$$\begin{aligned} TV(\hat{p}_{EL}, p_{e_0}) &= TV\left(\frac{\sum_s p(s, a_t, o_{t+1}|C_T)p(s|q_t)}{\sum_s p(s, a_t|C_T)p(s|q_t)}, \frac{\sum_s p(s, a_t, o_{t+1})p(s|q_t)}{\sum_s p(s, a_t)p(s|q_t)}\right) \\ &\leq \max_s TV\left(\frac{n(s, a_t, o_{t+1} \in C_T)}{n(s, a_t \in C_T)}, \frac{p(s, a_t, o_{t+1})}{p(s, a_t)}\right) \\ &\leq \underbrace{\sqrt{\frac{|O| \log(4|O|/\delta)}{n(s, a_t \in C_T)}}}_{\text{Hoeffding's inequality}} \text{ with probability at least } 1 - \delta/2 \\ &< \sqrt{\frac{2|O||S||A| \log(4|S|/\delta)}{T}} \text{ with probability at least } 1 - \delta \end{aligned}$$

This finishes the proof of Theorem 1

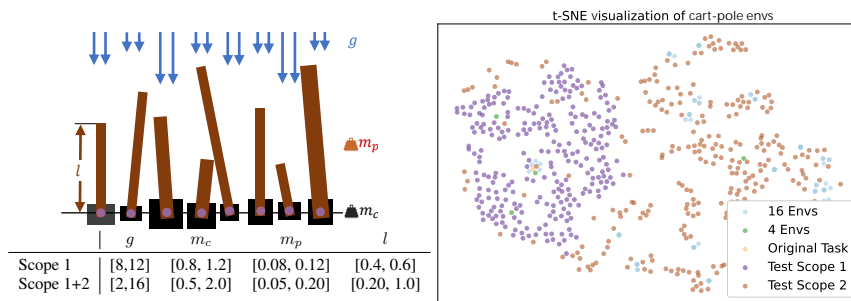
## B Additional Experiment Settings

### B.1 Environments and Datasets

**Cart-pole:** Figure 5 lists the scopes of the Cart-Pole environment variants, their t-SNE visualization, and details of the training and evaluation data. All datasets share a trajectory length of 200, which is sufficient for ICL in Cart-Pole variants. The training data comprises a total of 25.6M timesteps to avoid interference from data scale on performance, and the evaluation data contains 205K steps in total.

**Mazes:** Our maze environment is closely related to the settings described in Pašukonis et al. [70], Wang et al. [75], which are generated on a  $15 \times 15$  grid world. The distribution of the sampled mazes is shown in Figure 6 and Figure 7. The primary distinction between our mazes and those in previous work is the enhanced environmental diversity achieved through randomized configurations, which include the following:

- The textures of the ceiling, ground, and walls are randomly selected from a collection of 87 real-world textures.
- The scale of each grid varies from 1.5 m to 4.5 m, and the indoor height ranges from 2 m to 6 m.
- The ground clearance and the field of view (FOV) of the camera are varied between  $[1.6m, 2.0m]$  and  $[0.3\pi, 0.8\pi]$ , respectively.
- Two-wheeled dynamics are employed for the embodiment.



DataSets	# envs ( $ \mathcal{E} $ )	Len. Traj.	# Traj.	# time steps	Scope
1-Env	1	200	128K	25.6M	Original
4-Envs	4	200	32K	25.6M	Scope 1 & Scope 2
16-Envs	16	200	8K	25.6M	Scope 1 & Scope 2
8K-Envs (Scope 1)	8K	200	16	25.6M	Scope 1
8K-Envs (Scope 1+2)	8K	200	16	25.6M	Scope 1 & Scope 2
Evaluation (Scope 1)	256	200	4	205K	Scope 1
Evaluation (Scope 2)	256	200	4	205K	Scope 2
Evaluation (4-Envs)	4	200	256	205K	Scope 1 & Scope 2

Figure 5: Configuration scopes and cases of random Cart-Poles (upper left), t-SNE visualization of the configuration distribution (upper right), and a list of training and evaluation datasets.



Figure 6: bird's-eye view of 128 procedurally generated mazes in the Homogeneous dataset.

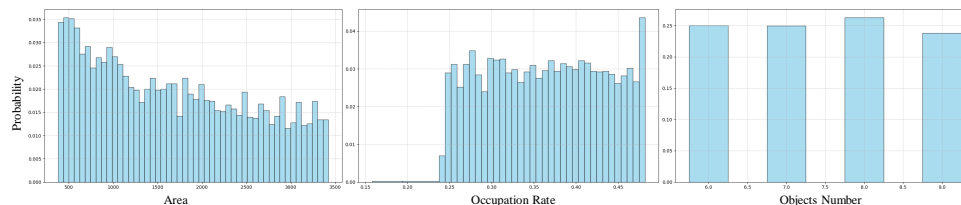


Figure 7: Distribution of the configurations (area, occupancy rate, and number of objects in each scene) in the 32K procedurally generated mazes

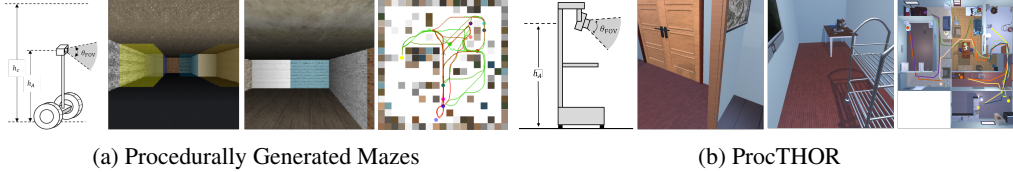


Figure 8: Illustration of the embodiment, the observation and the trajectories in procedurally generated mazes (a) and ProcTHOR (b).

Environments	Encoder & Decoder	$D$	$L$	$d$	$l_M$
Cart-pole	Raw	128	4	4	64
Navigation	Image	1024	18	32	64

Table 4: Model architecture and hyper-parameters for the two classes of environments

- Each environment involves  $[5, 15]$  objects, each marked with a crossable, translucent light wall of a different color.
- The agent receives a reward of 1.0 when reaching the goal, and a negative reward for collisions with walls, which is dependent on the agent’s speed.

**ProcTHOR:** We sample 336 training and 256 evaluating houses from the ProcTHOR-10K dataset. Unless otherwise specified, we keep both the trajectories and the environments of the validation datasets in ProcTHOR and Mazes separate from those of the training datasets. In seen-task validation, the environments have overlaps, but the trajectories are resampled.

## B.2 Details of Model Structures

The framework consists of the following modules:

- Observation Encoder (Image): A convolutional encoder that processes  $128 \times 128$  images into a  $D$ -dimensional latent vector through 9 convolution layers and 8 residual blocks.
- Observation Decoder (Image): A deconvolutional decoder that reconstructs  $128 \times 128$  images from a  $D$ -dimensional latent vector through 1 convolution layer, 8 residual blocks, and 3 transposed-convolution layers.
- Observation Encoder (Raw): A linear layer mapping from hidden size of 4 to  $D$ .
- Observation Decoder (Raw): A linear layer mapping from hidden size of  $D$  to 4.
- Latent Decoder: A 1-layer MLP with input size  $D$ , hidden size  $D$ , layer normalization, and residual connections.
- Action Encoder: A 1-layer MLP that encodes discrete actions into a  $D$ -dimensional hidden state.
- Sequence Decoder: A gated self-attention architecture with  $L$  layers, hidden size  $D$ , inner hidden size  $D$ ,  $d$  attention heads, memory length  $l_M$ , layer normalization, and block recurrence.

The hyper-parameters are specified as Table 4.

## B.3 Details of Training

All models were trained on NVIDIA A800 GPUs using the AdamW optimizer with the default settings in PyTorch [76].

**Cart-pole training details.** We train the model with a per-GPU batch size of 128, an epoch of 100, an initial learning rate of  $1.0e^{-4}$  and decayed to  $2.04e^{-5}$ .

**Maze pre-training details.** We first train the Image Encoder and Image Decoder with a per-GPU batch size of 400, an epoch of 50, and an initial learning rate of  $3e^{-4}$ . Subsequently, we train all

model components with a per-GPU batch size of 10, an epoch of 10, an initial learning rate of  $2.0e^{-4}$ , and decayed to  $8.8e^{-5}$ .

**ProcTHOR training details.** We first train the Image Encoder and Image Decoder using the same settings as in Maze pretraining, except for the initial learning rate, which is set to  $2.0e^{-4}$ . The VAE is then frozen, while the remaining modules are initialized from the weights trained on the Maze dataset and further fine-tuned on ProcThor data. For the 40k version of ProcThor, we train for 10 epochs with a per-GPU batch size of 10 and an initial learning rate of  $2.0e^{-4}$ , decayed to  $1.2e^{-4}$ . For the 5k version, we use the same settings but train for 20 epochs.

## C Additional Results

**Additional results of the performances of L2World in Mazes.** Table 5 presents the prediction error (measured as the mean square error between observations) of L2World and the other baselines on the Maze datasets. The prediction errors are fully consistent with the PSNR evaluation; therefore, we report only the PSNR results in the remaining experiments. Table 6 details the K-step prediction performance, corresponding to the histograms in Figure 3.

Table 5: 1-step prediction error( $\downarrow$ ) of different world models in Mazes.

Model	Seen					Unseen				
	T=1	T=10	T=100	T=1000	T=10000	T=1	T=10	T=100	T=1000	T=10000
L2World (Maze-32K-L)	2.09e-02	8.01e-03	4.89e-03	3.43e-03	3.13e-03	2.30e-02	<b>7.51e-03</b>	<b>4.82e-03</b>	<b>3.42e-03</b>	<b>3.42e-03</b>
L2World (Maze-32K-S)	1.39e-02	1.18e-02	1.08e-02	9.53e-03	8.96e-03	<b>1.43e-02</b>	1.19e-02	1.09e-02	9.35e-03	9.31e-03
L2World (Maze-128-S)	1.13e-02	9.15e-03	8.74e-03	6.28e-03	6.66e-03	1.58e-02	1.37e-02	1.26e-02	1.08e-02	1.09e-02
L2World (Maze-128-L)	1.40e-02	8.20e-03	<b>4.66e-03</b>	<b>2.72e-03</b>	<b>2.51e-03</b>	1.76e-02	1.14e-02	8.02e-03	7.01e-03	7.04e-03
Dreamer (Maze-32K-L)	2.29e-02	<b>6.57e-03</b>	1.19e-02	7.47e-03	6.47e-03	2.08e-02	8.95e-03	7.25e-03	5.43e-03	6.14e-03
Dreamer (Maze-128-L)	1.94e-02	8.63e-03	6.56e-03	6.02e-03	5.72e-03	3.75e-02	3.51e-02	3.90e-02	4.50e-02	4.46e-02
NWM (Maze-32K-L)	<b>8.22e-03</b>	9.52e-03	1.20e-02	5.86e-03	7.83e-03	2.02e-02	2.26e-02	2.48e-02	1.70e-02	1.28e-02

Table 6: Average PSNR of  $k$ -Step auto-regressive prediction in Mazes (Unseen).

Model	T=1				T=10				T=100				T=1000				T=10000			
	k=1	k=2	k=4	k=8																
L2World (Maze-32K-L)	16.94	15.79	14.74	13.39	<b>21.02</b>	<b>19.88</b>	<b>18.96</b>	15.83	<b>23.24</b>	<b>22.16</b>	<b>20.85</b>	<b>18.31</b>	<b>24.60</b>	<b>23.57</b>	<b>21.33</b>	<b>18.03</b>	<b>24.80</b>	<b>24.11</b>	<b>21.81</b>	<b>18.72</b>
L2World (Maze-32K-S)	<b>18.44</b>	<b>17.41</b>	<b>16.82</b>	<b>15.61</b>	19.23	19.05	17.92	<b>16.73</b>	19.62	19.43	18.19	16.69	20.29	20.17	18.89	17.03	20.31	20.21	18.83	17.00
L2World (Maze-128-S)	18.00	16.83	16.23	15.17	18.62	18.18	17.06	15.96	18.98	18.53	17.39	15.93	19.65	19.09	17.86	16.10	19.62	19.12	17.91	16.18
L2World (Maze-128-L)	17.53	15.99	15.38	14.53	19.45	18.73	17.67	16.64	20.96	20.47	19.11	17.57	21.54	20.76	19.45	17.48	21.53	21.05	19.58	17.65
Dreamer (Maze-32K-L)	16.16	15.80	14.62	13.12	19.66	18.96	17.72	16.25	21.89	20.99	20.33	17.74	23.13	22.08	20.57	17.00	23.16	21.85	20.23	16.14
NWM (Maze-32K-L)	16.20	13.37	11.68	11.16	16.71	13.34	11.65	11.00	17.00	13.86	12.13	11.48	17.37	13.82	12.24	12.60	17.85	14.51	12.60	12.46

**ICEL and ICER in navigation world models implicitly perform global mapping.** We further show that predicting transitions alone, without any specifically designed tasks, can potentially capture the global map implicitly. We collect 12 trajectories from 4 unseen mazes (3 trajectories in each maze) and track the transformation of memory states ( $\phi_t$ ) across each of the linear attention layers. Among the 18 layers used in the transition model, we select layers  $\{1, 6, 12, 18\}$  for t-SNE visualization of the memory states ( $\phi_t$ ). To ensure that the 4 unseen mazes are not trivially discriminable, for instance, by geometric and embodiment configurations in one-shot, we maintain identical configurations for most aspects of the evaluated 4 mazes while varying only their topology, such as the arrangement of walls. We employ silhouette scores [77] to quantify clustering quality, where higher values indicate better environment separation. As visualized in Figure 10, we highlight two insights: first, training solely on transition prediction across diverse environments and long contextual windows implicitly learns a spatial map, potentially removing the need for auxiliary mapping modules; second, ICEL and ICER behave differently across layers, suggesting distinct underlying mechanisms.

**Investigating ICEL from perspectives of predictive coding.** The concept of predictive coding has emerged as a foundational mechanism in both biological and artificial learning systems [24], in which the discrepancy between expected and observed outcomes drives attention and learning. To investigate the correlation between ICEL and predictive coding, we conducted experiments to examine how prediction error influences learning progress. Specifically, we selected three positions  $T = \{10, 100, 1000\}$  for each of 256 evaluating sequences. At these positions, we replaced the ground-truth observations  $s_t$  with model-generated predictions, thereby suppressing error-correction signals derived from real-world feedback. We then compared the accuracy loss in subsequent frames (including  $k = 1$  and  $k = 8$ ) with and without this replacement. This comparison quantifies the importance of ground-truth observations for learning progress. As illustrated in Figure 9, we observed

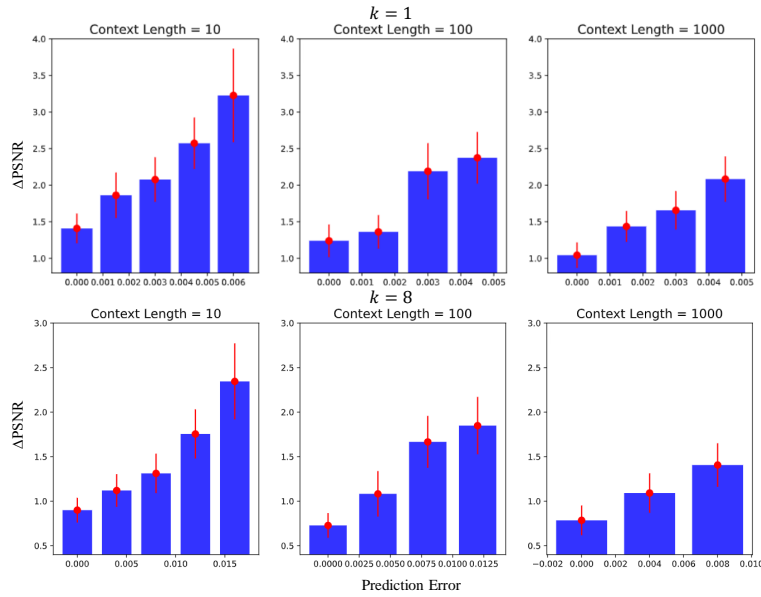


Figure 9: We investigated the correlation between the average prediction error and the performance change. The performance change was quantified by  $\Delta\text{PSNR}$ .  $\Delta\text{PSNR}$  is acquired by the loss of accuracy by replacing the input  $s_t$  with predicted  $\hat{s}_t$  and then measuring the loss of PSNR in future predictions with  $k = 1$  and  $k = 8$ .

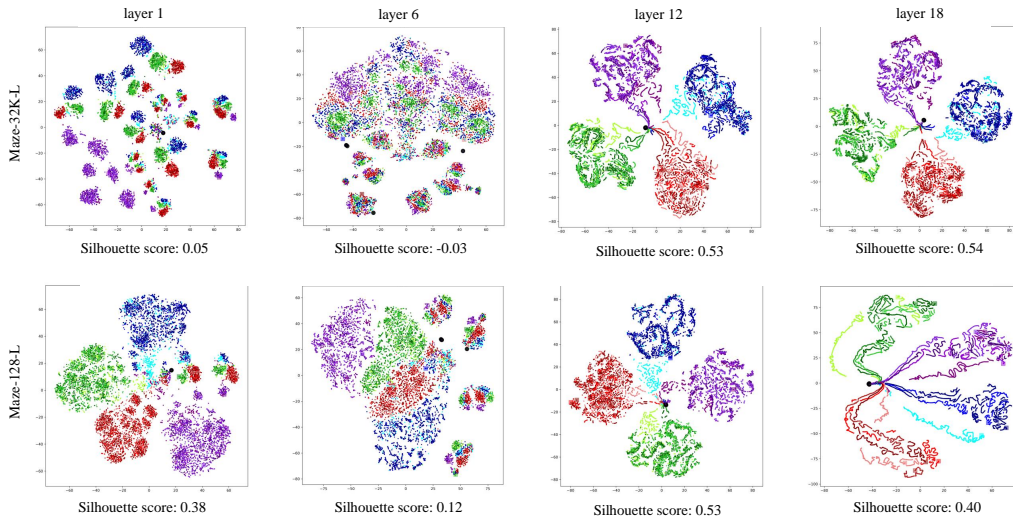


Figure 10: t-SNE visualization of the memory states  $\phi_t$  in state transition prediction for Maze-32K-L and Maze-128-L groups. We visualize the memory states from layers 1, 6, 12, and 18. The visualization encompasses 12 trajectories across 4 distinct environments that are similar yet exhibit slight differences. Trajectories originating from the same environment are indicated by similar colors. The Silhouette score is computed by treating trajectories from each environment as individual classes.

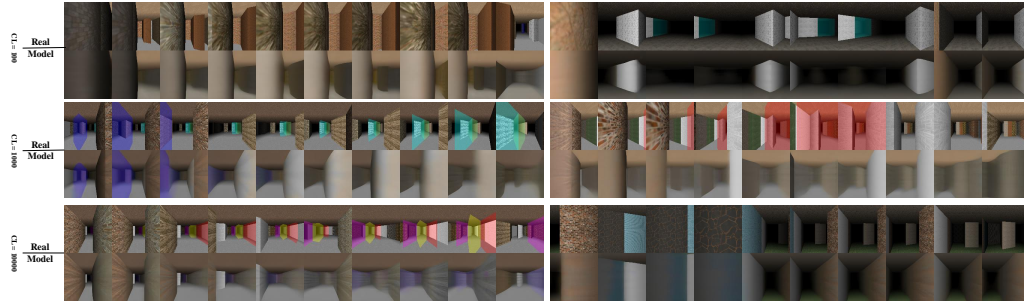
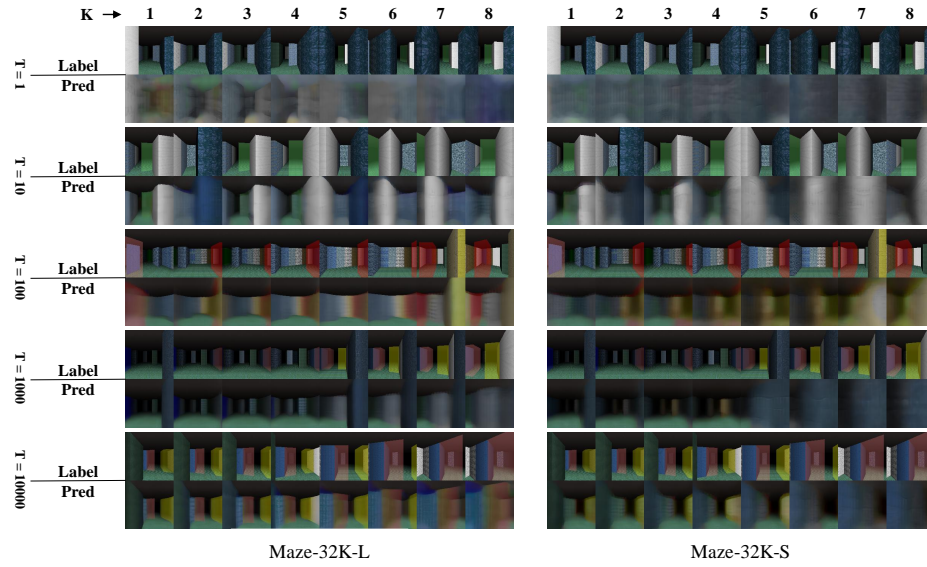


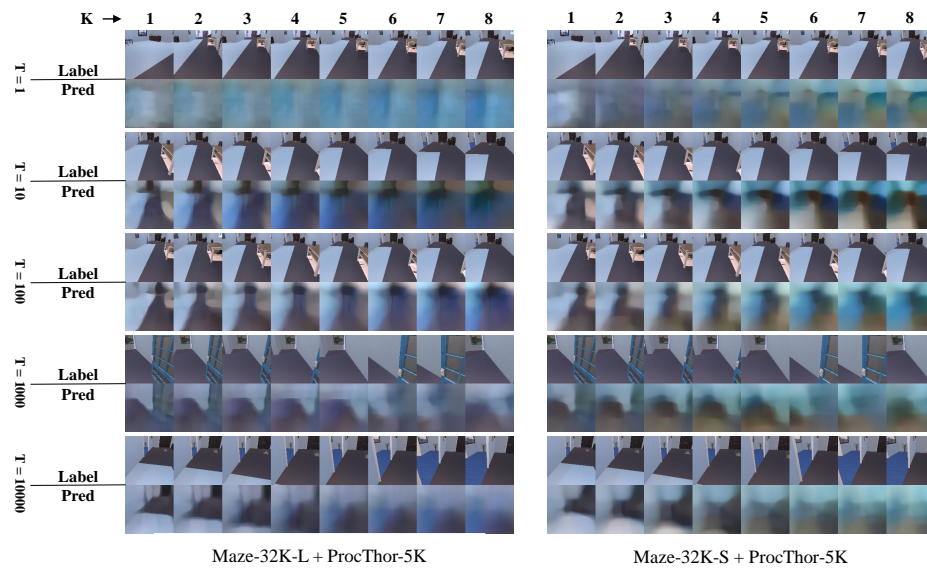
Figure 11: 2 failed examples produced by L2World on Mazes with  $T = \{1, 100, 10000\}$  and  $k = 8$ .

a clear positive correlation between the mean performance difference ( $\Delta\text{PSNR}$ ) and the prediction error (MSE loss) of the replaced frame. This finding suggests that ICEL progress is sensitive to prediction error, a phenomenon reminiscent of predictive coding in biological systems. These results further validate ICL as a prospective mechanism for adapting world models to variant environments.

**Additional Cases.** Figure 11 shows two failure predictions of L2World (Maze-32K-L) on unseen maze environments. These failures appear to stem from excessive blurring in the predictions, which causes the compound error to explode rapidly as  $k$  increases. Building on this observation, a natural extension of our work is to inject additional overshooting during training so that the world model can better forecast distant futures. Figure 12 juxtaposes the performance of L2World trained with 32K-L and 32K-S, clearly evidencing the benefit of longer sequences in incentivizing ICEL.



(a) Maze



(b) ProcThor

Figure 12: Example predictions by L2World trained with Maze-32K-L and Maze-32K-S at  $T = \{1, 10, 100, 1000, 10000\}$  and  $k = 8$ .